Electronic structure and EPC stability of the α-Sn/InSb(111)A nonpolar-polar heterojunction interface

Kazuo Yamamoto and Kazuaki Kobayashi
National Institute for Research in Inorganic Materials, 1-1 Namiki, Tsukuba, Ibaraki 305, Japan
(Received September 5 1995; revised manuscript received 24 October 1995)

The electronic structures and stability of the α-Sn/InSb(111)A nonpolar-polar interface are investigated with use of first-principles norm-conserving pseudopotential calculations. An ideally abrupt α-Sn/InSb(111)A interface is formed by only a Sn-In bond. According to the simple bond-charge picture, a charge of this bond is depleted by 0.25 electron. This leads to the formation of a macroscopic electric field, to make the interface unstable. In order to neutralize the charge at the interface, we have proposed an interface model. Our calculations show that as a Sn atom buries the In-vacancy site in the vacancy-buckled surface of InSb(111)A-(2×2), a coherent interface becomes more stable and the electric field is depressed.

I. INTRODUCTION

Heterojunction interfaces between different semiconductor materials hold significant potential for technological applications and have been the subject of extensive experimental and theoretical studies.[1–17] Of particular interest is the heterovalent interface between a group-IV elemental semiconductor (A^{IV}) and a III-V compound semiconductor ($B^{III}C^{V}$) with the aim of incorporation of optoelectronics into microelectronics. This interface contains A^{IV}-B^{III} and/or A^{IV}-C^{V} bonds. According to a simple bond-charge picture, each bond in the tetrahedrally coordinated structure has exactly two electrons, as in the A^{IV}-A^{IV} and B^{III}-C^{V} bonds. Therefore the charge of the A^{IV}-B^{III}(A^{IV}-C^{V}) bond is depleted (exceeded) by 0.25 electron. A classical electrostatic treatment by Harrison *et al.* showed that for the polar {100} and {111} orientations of the ideally abrupt $A^{IV}/B^{III}C^{V}$ interfaces, which are formed by only the A^{IV}-B^{III}or A^{IV}-C^{V} bond, this electrically charged defect creates a macroscopic electric field along the interface normal, to make the interfaces unstable.[5] They introduced interfacial reconstructions that can reduce the macroscopic electric field. However, it is unclear how the interfacial reconstructions emerge.

Recently, considerable attention has been devoted to heterostructure of α-Sn/InSb.[18–23] α-Sn has a band gap nearly equal to zero (0.08 eV at 300 K), while InSb has a wider band gap (0.17 eV at 300 K). Thus the heterostructure of α-Sn/InSb is a candidate for light-emitting and far-infrared laser devices. α-Sn, which is thermodynamically stable below 13.2 °C, can grow heteroepitaxially above room temperature on lattice-matched crystals of InSb.[19,20,24] Some factors that dominate the formation of the metastable α-Sn films on InSb are discussed in a previous paper.[19] One is strong interfacial chemical bonding between α-Sn and InSb, the other extremely the small lattice misfit between them (0.14%).

In this paper, we focus our attention on electronic structures and stability of the α-Sn/InSb(111)A nonpolar-polar interface in terms of the above-mentioned electrical neutrality of the charged defect at the interface. We have already proposed an interfacial reconstruction that is deduced from the experimental facts.[19] Our first-principles calculations show that as a Sn atom buries the In-vacancy site in the vacancy-buckled surface of InSb(111)A-(2×2), a coherent interface becomes more stable and the electric field is depressed.

II. MODELS AND METHOD OF CALCULATION

Reflection high-energy electron diffraction (RHEED) and Auger electron spectroscopy experiments for the α-Sn/InSb{111} system have established the following information:[18,19] α-Sn thin films grow with a biatomic layer-by-layer mode on InSb(111)A and with a more complicated layerlike mode accompanied by Sb segregation on InSb(111)B. The difference in the growth mode is due to that in the predeposited surface structure between an InSb(111)A-(2×2) substrate and an InSb(111)B-(2×2) substrate. As is well established, the surface structure of InSb(111)A-(2×2) is the vacancy buckling structure where 0.25 monolayer (ML) of In is missing at the outermost surface and subsurface Sb atoms around the In vacancy are relaxed.[25] On the other hand, the surface structure of InSb(111)B-(2×2) is the Sb-trimer adsorption structure where the trimer is located at a fourfold atop site of the outermost Sb layer.[26] The adsorbed trimer brings about the Sb segregation into the Sn layers. In this paper we deal with the α-Sn/InSb(111)A system, which is less complicated than the α-Sn/InSb(111)B system.

As mentioned in the Introduction, if the first atomic plane adjacent to the α-Sn layers were a perfect In plane, the defect charge of the nanoctet Sn-In bond, +0.25 electron, is accumulated at the interface, causing a macroscopic electric field. This electric field is roughly estimated at $E=4\pi\sigma/\varepsilon=1.6\times10^{7}$ V/cm, where σ is the areal defect charge density and ε is the dielectric constant of InSb. In order to neutralize the charge at the interface, therefore, redistribution of the charge and/or atomic rearrangements from the ideally abrupt planar interface are inevitable. We have already introduced a reconstructed interface model, as shown in Fig. 1(a), on the basis of the experimental fact:[19] At the initial stage of Sn growth on the InSb(111)A-(2×2) surface, 0.25 ML of Sn deposition gives the (1×1) structure, followed by a biatomic layer-by-layer growth of Sn. Considering that the atomic scattering

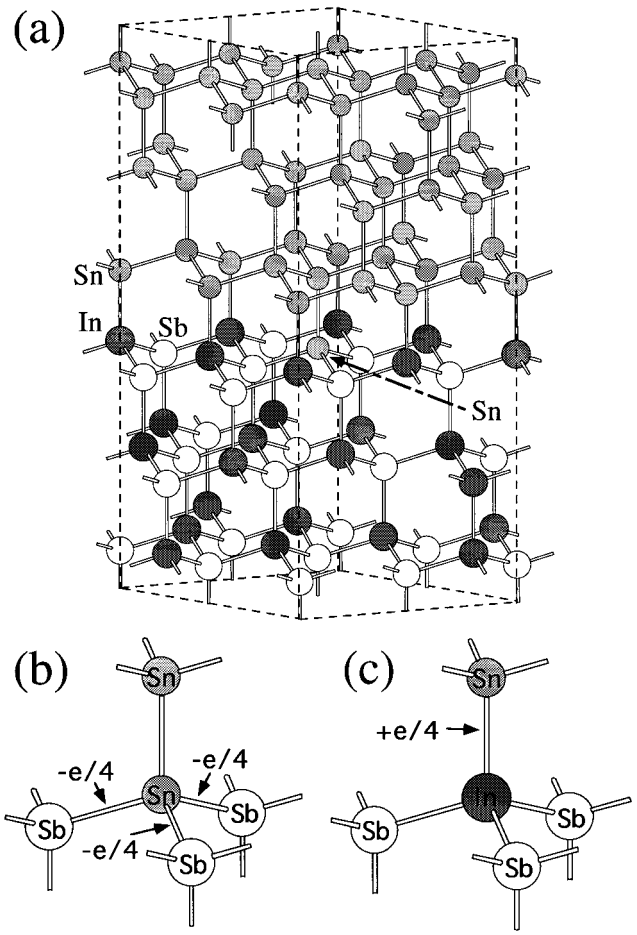

FIG. 1. (a) Schematic representation of the supercell of the α-Sn/InSb(111)A-(2×2) reconstructed interface model employed in the present calculations. The (111)A interface is formed as a Sn atom buries the In-vacancy site in the vacancy buckling structure of the InSb(111)A-(2×2) surface followed by a biatomic layer-by-layer growth of α-Sn. For the case of the ideal interface model a Sn atom embedded in the vacancy site in InSb(111)A-(2×2) is replaced by an In atom. (b) An enlargement of Sb-Sn bonds, at the (111)A interface, which have a defected charge $-0.25e$. (c) An enlargement of In-Sn bonds, at the (111)A interface, which have a defected charge $+0.25e$. The number of the Sb-Sn bonds is 3 per (2×2) areal unit cell and equals that of the In-Sn bonds.

factor of In ($Z=49$, where Z is the atomic number) is extremely close to that of Sn ($Z=50$), if 0.25 ML of Sn completely buries the In-vacancy site of the InSb(111)A-2×2 surface, the (1×1) reflection can be observed in the RHEED pattern. In this reconstructed interface model the number of the Sn-In bonds is 3 per the (2×2) areal unit cell and equals that of the Sn-Sb bonds at the interface [Figs. 1(b) and 1(c)], so that the neutralization of the defect charges is achieved.

In the present calculations we have employed a supercell geometry that is periodically repeated in the direction perpendicular to the interface as well as in the plane parallel to the interface. Figure 1(a) illustrates this supercell configuration for the α-Sn/InSb(111)A reconstructed interface. The supercell has two 2×2 interfaces and consists of three biatomic Sn layers and three biatomic InSb layers including a Sn atom embedded in the In-vacancy site of InSb(111)A-(2×2). Each layer has four atoms. Since the lattice misfit between InSb and α-Sn is extremely small, we used the experimental lattice constant of zinc-blende InSb, 6.48 Å, for both the InSb layers and the α-Sb layers and did not optimize the geometry of the supercell. For comparison we have also studied the electronic structure of the α-Sn/InSb(111)A ideally abrupt planar interface (hereafter referred to as the ideal interface). The supercell of the ideal interface was obtained by replacing the vacancy-site Sn atom of the reconstructed model with an In atom. Both the reconstructed interface model and the ideal interface model have the α-Sn/InSb(111)B interface as well as the α-Sn/InSb(111)A interface because of the repeating slab geometry. As stated above, the detailed atomic structure of the α-Sn/InSb(111)B interface is not clear since Sb segregates into the Sn layers. Therefore we adopted the ideally abrupt planar arrangement for the α-Sn/InSb(111)B interface part of both the models. We paid attention mainly to the α-Sn/InSb(111)A interface part.

Our calculation[27] is based on the local-density approximation in density-functional theory[28,29] with the Wigner interpolation formula[30] for the exchange-correlation and a norm-conserving pseudopotential. As for In, Sn, and Sb pseudopotentials, the optimized pseudopotentials originated from Troullier and Martin[31] were used in order to reduce a number of plane waves. Nonlocal parts of s and p pseudopotentials were transformed to the Kleinman-Bylander separable form.[32] In addition, we introduced a partial core correction[33] (PCC) to the In pseudopotential in order to consider a nonlinear effect for the exchange-correlation term in a shallow $4d$ core state. No ghost bands by these treatments were found in this study. A term of spin-orbit interaction was not considered in this band structure calculation.

We performed preliminary calculations for bulk In, InSb, and α-Sn to check the pseudopotentials. Without taking account of the PCC, the lattice constant of fcc In is 6.7% smaller and the bulk modulus is 71% larger than the other all-electron calculation lattice constant $a_0^{\mathrm{In}}=4.74$ Å (Ref. 34) and the all-electron calculation bulk modulus of 0.35 Mbar,[34] respectively. Applying the PCC, the deviations of the lattice constant and the bulk modulus are reduced to 2.5% and 23%, respectively. Although the PCC can be neglected for Sn and Sb, it is very important for In. The experimental lattice constants of InSb ($a_0^{\mathrm{InSb}}=6.480$ Å) and α-Sn ($a_0^{\alpha\text{-Sn}}=6.489$ Å) are well reproduced with errors of 0.6% and 0.1%, respectively. The calculated bulk moduli of InSb and α-Sn are 0.52 and 0.43 Mbar, which deviate from the experimental bulk moduli $B^{\mathrm{InSb}}=0.46$ Mbar (Ref. 35) and $B^{\alpha\text{-Sn}}=0.54$ Mbar (Ref. 36) with errors of 13% and 20%, respectively.

We have adopted a plane-wave basis set for the wave-function expansion. The cutoff energy of the plane-wave basis is 16 Ry, which results in a maximum number of 11 964 plane waves for both the models. The Brillouin zone is divided into 2×2×2 meshes and eight inequivalent k points are used.

III. RESULTS AND DISCUSSION

In order to clarify the properties of heterojunction interfaces, information on the variation of the two-dimensional (xy-planar) average of electronic states along the interface normal (z axis) is indispensable. We first introduce the

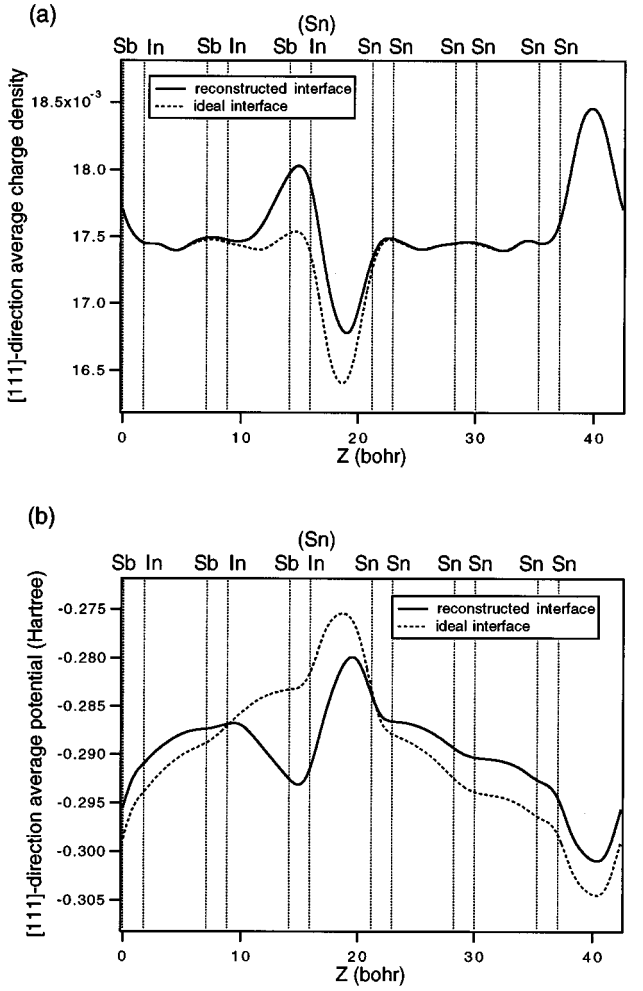

FIG. 2. [111] direction macroscopic averages of (a) the charge densities and (b) the total potentials for the α-Sn/InSb(111)*A* reconstructed interface model (solid lines) and the ideal interface model (broken lines). The total potential is the sum of the Coulomb, the exchange-correlation, and the local pseudopotential.

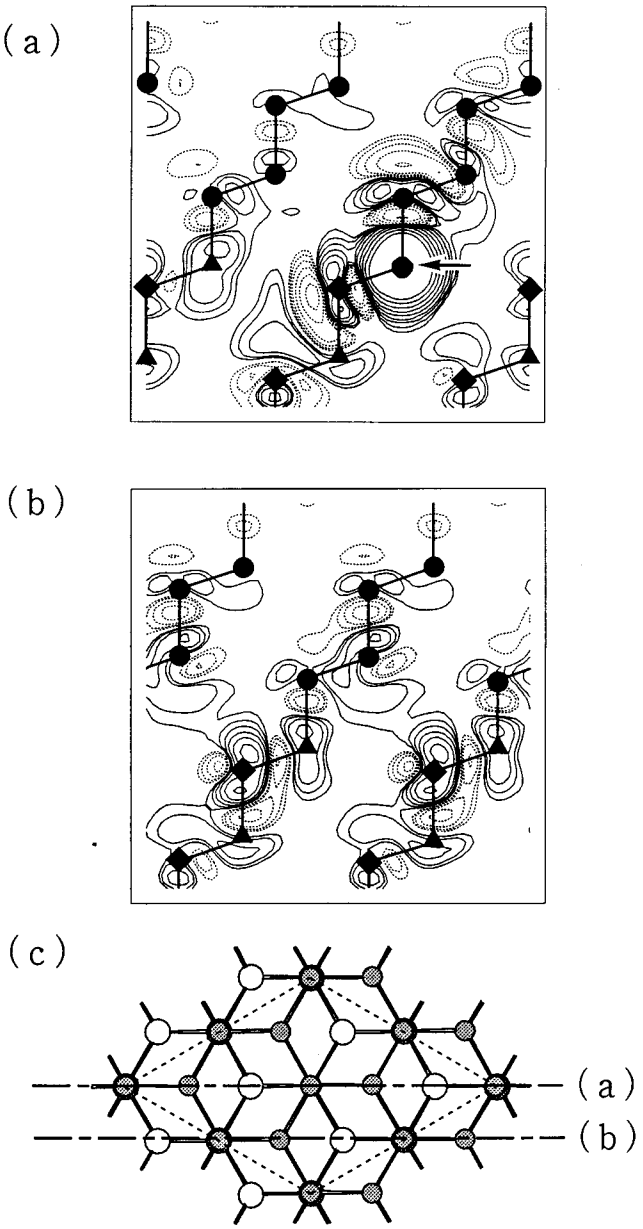

FIG. 3. Contour maps of difference charge density $\Delta\rho=\rho$ (the reconstructed interface model) $-\rho$ (the ideal interface model). The contours (a) and (b) are drawn for the (110) plane normal to the interface, including the dash-dotted lines (a) and (b), respectively, in the top view of the (2×2) areal unit cell (c). In (a) and (b) the solid and the dotted lines indicate the amount of the accumulated and the depleted charges, respectively. Solid circles, solid triangle, and solid square denote Sn, In, and Sb atoms, respectively. The atom marked by an arrow in (a) is the vacancy site atom in the InSb(111)*A*-(2×2).

xy-planar average of the calculated self-consistent charge density $\rho(x,y,z)$ or total potential $V(x,y,z)$,

$$f(z)=\frac{1}{A}\int\int_{A} f(x,y,z)\,dx\,dy, \tag{1}$$

where f refers to the charge density ρ or the total potential V and A is the area of the two-dimensional unit cell. The total potential is the sum of the Coulomb, the exchange-correlation, and the local pseudopotential. Both the planar-averaged charge densities and the total potentials for the α-Sn/InSb(111)*A* reconstructed interface model and the ideal interface model display strong oscillations. The behavior of the oscillations, in which positions of the higher charge densities are at the InSb and Sn bilayers and correspond to those of the lower total potentials, is bulklike and makes it difficult to distinguish an interface effect such as the macroscopic electric field across the interface. The difference in the planar-averaged total potential and charge density between the reconstructed interface model and the ideal interface model is barely visible near the interface. Therefore, we have adopted the one-dimensional macroscopic average of $f(z)$ over a period centered at z,

TABLE I. Total energies and interface adhesion energies for the reconstructed interface model and the ideal interface model. The total energies of the constituent parts of both these models are calculated in the same unit cell size, number of k points, and cutoff energies as the α-Sn/InSb(111) models.

Energy (hartree)	Reconstructed interface model	Ideal interface model
E_T [α-Sn/InSb(111)]	−179.584	−178.146
E_T (α-Sn layers)	−85.212	−85.212
E_T (InSb layers including vacancy)	−90.309	−90.309
E_T (vacancy site atom)	−3.402 (Sn)	−2.007 (In)
Interface adhesion energy ΔE_A	−0.661	−0.618

$$\overline{f(z)}=\frac{1}{d}\int_{z-d/2}^{z+d/2} f(z')dz', \tag{2}$$

where d is the interplanar spacing in the z direction.[14] We present in Figs. 2(a) and 2(b) the [111] direction macroscopic averages of the charge densities and the total potentials, respectively, for the reconstructed interface model and the ideal interface model. As shown in Fig. 2, the variations of the charge densities and the potentials at the In/Sn [α-Sn/InSb(111)A] interface and the Sb/Sn [α-Sn/InSb(111)B] interface are remarkable. We can easily distinguish the difference in the behavior of the charge density and the potential between the reconstructed interface and the ideal interface. For the ideal interface model the charge density has the lowest value at the In/Sn interface and the highest value at the Sb/Sn interface [see the broken line in Fig. 2(a)]. Owing to this interface charging, the potential falls right down from the highest value at the In/Sn interface to the lowest value at the Sb/Sn interface in both the InSb layers and the Sn layers [broken line in Fig. 2(b)]. On the other hand, the charge density around the In/Sn interface of the reconstructed interface model [solid line in Fig. 2(a)] is higher than that of the ideal interface model because $\frac{1}{4}$ ML of In at the interface is replaced by $\frac{1}{4}$ ML of Sn. This is reflected in the profile of the potential, indicated by the solid line in Fig. 2(b), whose maximum near the In/Sn interface is lowered and whose decrease from the maximum to the minimum at the Sb/Sn interface is slow compared with that of the ideal interface model. Although the charge densities around the Sb/Sn interface of both the models are almost the same, the potential around the Sb/Sn interface of the reconstructed interface model is lower than that of the ideal interface model. Considering that the atomic geometries of the Sb/Sn interface of both the models are the same, the potential is strongly affected by the long-range electrostatic interaction due to the defect charge at the In/Sn interface far away from the Sb/Sn interface. The overall features of Fig. 2(b) show that the gradient of the [111] direction macroscopic average of the total potential for the reconstructed interface model is slower than that for the ideal interface model. The gradient of the potential is equivalent to a macroscopic electric field. We estimated the macroscopic electric fields of both the models. The values at the center of the InSb layer are 6×10^6 and 1×10^6 V/cm, respectively. The former value is in agreement with the above-mentioned roughly estimated value for the ideally abrupt interface. Therefore, the macroscopic electric field is depressed when the reconstructed interface, in which a Sn atom buries the In-vacancy site in the vacancy-buckled surface of InSb(111)A-(2×2), is formed. This result suggests that the reconstructed interface becomes more stable than the ideal interface.

In order to discuss quantitatively the stability of the interfaces with different stoichiometry, we define the interface adhesion energy

$$\begin{aligned}\Delta E_A = {} & E_T[\alpha\text{-Sn/InSb}(111)] - \{E_T(\alpha\text{-Sn three bilayers} \\ & + \text{vacuum three bilayers}) \\ & + E_T(\text{InSb three bilayers including vacancy} \\ & + \text{vacuum three bilayers}) \\ & + E_T(\text{vacancy-site atom} + \text{vacuum})\},\end{aligned} \tag{3}$$

where the total energies of the constituent part E_T(α-Sn three bilayers+vacuum three bilayers), E_T(InSb) three bilayers including vacancy+vacuum three bilayers), and E_T (vacancy-site atom+vacuum) are calculated in the same unit cell size, number of k points, and cutoff energies as E_T[α-Sn/InSb(111)]. Each constituent part includes surfaces. The adhesion energy refers to the energy gain owing to bond formation at the interface, the electric-field depression, and so on. The calculated adhesion energies of the reconstructed interface model and the ideal interface model are given in Table I. The results show that the reconstructed interface model is energetically more favorable than the ideal interface model by 1.2 eV/unit cell (0.043 hartree/unit cell).

We discuss the redistribution of the charge as well as the atomic rearrangements from the ideally abrupt planar interface in order to attain the neutralization of the defected charges at the interface. Figure 3 shows contour maps of the difference charge density $\Delta\rho=\rho$(reconstructed interface model)-ρ(ideal interface model), which is drawn for the (110) plane normal to the interface. In this figure, the charge increment around the vacancy site atom is remarkable because of replacing the In atom in the ideal interface model by the Sn atom in the reconstructed interface model. However, the extra charge is not localized there but transferred to the remaining atoms and/or bonds around the interface. This is also seen in the [111] direction macroscopic averages of the charge densities shown in Fig. 2(a). As a result of the charge redistribution as well as the interface reconstruction, the in-

duced macroscopic electric field along the interface normal is depressed, leading to making the interface stable.

Recently, Ohtake, Omi, and Osaka studied dynamical growth processes of α-Sn films on the InSb(111)*A*-(2×2) substrate by using a RHEED oscillation technique. Their detailed analysis has shown that the present reconstructed interface model is reasonable from the experimental fact that the RHEED oscillation intensity does not decrease but increase at the initial growth stage of α-Sn below 0.25 ML.[37]

IV. CONCLUSION

First-principles norm-conserving pseudopotential calculations have been performed to investigate the electronic structures and stability of the α-Sn/InSb(111)*A* nonpolar-polar interface. In order to achieve the neutralization of the defected charges emerged at the nonpolar-polar interface, we have proposed the α-Sn/InSb(111)*A* reconstructed interface model. By comparing the potential profile of the reconstructed interface model with that of the ideally abrupt interface model, it is concluded that the macroscopic electric field due to the defected charge is lowered for the reconstructed interface model. Our total-energy calculations show that the reconstructed interface model is more stable than the ideal interface model. Our results support the reconstructed interface deduced from the experimental facts.

ACKNOWLEDGMENTS

We are indebted to Dr. T. Aizawa and Dr. Y. Uemura for a critical reading of this manuscript and for valuable comments. We gratefully acknowledge helpful discussions with Professor T. Osaka of Waseda University. We wish to thank Dr. T. Nakada, Dr. H. Omi, A. Ohtake, and S. Suehara for valuable suggestions and comments. The calculations were partially performed on the FACOM VPP500 at the Supercomputer Center, Institute for Solid State Physics, University of Tokyo.

[1] E. A. Kraut, R. W. Grant, J. R. Waldrop, and S. P. Kowalczyk, Phys. Rev. Lett. **44**, 1620 (1980).
[2] H. Brugger, F. Schäffler, and G. Abstreiter, Phys. Rev. Lett. **52**, 141 (1984).
[3] G. Margaritondo, Surf. Sci. **168**, 439 (1986).
[4] R. S. Bauer and G. Margaritondo, Phys. Today **40** (1), 26 (1987).
[5] W. A. Harrison, E. A. Kraut, J. R. Waldrop, and R. W. Grant, Phys. Rev. B **18**, 4402 (1978).
[6] H. Kroemer, J. Cryst. Growth **81**, 193 (1987); Surf. Sci. **132**, 543 (1983).
[7] J. E. Northrup, R. D. Bringans, R. I. G. Uhrberg, M. A. Olmstead, and R. Z. Bachrach, Phys. Rev. Lett. **61**, 2957 (1988).
[8] G. A. Baraff, J. A. Appelbaum, and D. R. Hamann, Phys. Rev. Lett. **38**, 237 (1977); J. Vac. Sci. Technol. **14**, 999 (1977).
[9] C. G. Van de Walle and R. M. Martin, Phys. Rev. B **34**, 5621 (1989); **35**, 8154 (1987).
[10] D. M. Bylander and L. Kleinman, Phys. Rev. Lett. **59**, 2091 (1987); Phys. Rev. B **36**, 3229 (1987); **34**, 5280 (1986); **39**, 5116 (1989); **41**, 3509 (1990).
[11] A. Muñoz, N. Chetty, and R. M. Martin, Phys. Rev. B **41**, 2976 (1990); N. Chetty and R. M. Martin, *ibid.* **45**, 6089 (1992).
[12] I. P. Batra, S. Ciraci, and E. Özbay, Phys. Rev. B **44**, 5550 (1991); S. Ciraci and I. P. Batra, *ibid.* **38**, 1835 (1988).
[13] T. Ohno and T. Ito, Phys. Rev. B **47**, 16 336 (1993).
[14] A. Baldereschi, S. Baroni, and R. Resta, Phys. Rev. Lett. **61**, 734 (1988).
[15] A. Continenza and A. J. Freeman, Phys. Rev. B **45**, 5953 (1992).
[16] A. Kley and J. Neugebauer, Phys. Rev. B **50**, 8616 (1994).
[17] W. R. L. Lambrecht and B. Segall, Phys. Rev. B **41**, 2832 (1990); W. R. L. Lambrecht, B. Segall, and O. K. Andersen, *ibid.* **41**, 2813 (1990).
[18] H. Omi, H. Saito, and T. Osaka, Phys. Rev. Lett. **72**, 2596 (1994).
[19] T. Osaka, H. Omi, K. Yamamoto, and A. Ohtake, Phys. Rev. B **50**, 7567 (1994).
[20] Y. Kasukabe, M. Iwai, and T. Osaka, Jpn. J. Appl. Phys. **27**, L1201 (1988).
[21] P. John, T. Miller, and T.-C. Chang, Phys. Rev. B **39**, 3223 (1989).
[22] H. Höchst and I. H. Calderon, J. Vac. Sci. Technol. A **3**, 911 (1985); Surf. Sci. **126**, 25 (1981); I. H. Calderon and H. Höchst, *ibid.* **152/153**, 1035 (1985).
[23] A. Förster, A. Tulke, and H. Lüth, J. Vac. Sci. Technol. B **5**, 1054 (1987).
[24] R. F. C. Farrow, D. S. Robertson, G. M. Williams, A. G. Cullis, G. R. Jones, I. M. Young, and P. N. J. Dennis, J. Cryst. Growth **54**, 507 (1981).
[25] J. Bohr, R. Feidenhans'l, M. Nielsen, M. Tony, R. L. Johnson, and I. K. Robinson, Phys. Rev. Lett. **54**, 1275 (1985).
[26] T. Nakada and T. Osaka, Phys. Rev. Lett. **67**, 2834 (1991).
[27] K. Kobayashi, Y. Morikawa, K. Terakura, and S. Blügel, Phys. Rev. B **45**, 3469 (1992).
[28] P. Hohenberg and W. Kohn, Phys. Rev. **136**, B864 (1964).
[29] W. Kohn and L. J. Sham, Phys. Rev. **140**, A1133 (1965).
[30] E. Wigner, Phys. Rev. **46**, 1002 (1934).
[31] N. Troullier and J. L. Martin, Solid State Commun. **74**, 613 (1990); Phys. Rev. B **43**, 1193 (1991).
[32] L. Kleinman and D. M. Bylander, Phys. Rev. Lett. **48**, 1425 (1983).
[33] S. G. Louie, S. Froyen, and M. L. Cohen, Phys. Rev. B **26**, 1738 (1982).
[34] V. L. Moruzzi, J. F. Janak, and A. R. Williams, *Calculated Electronic Properties of Metals* (Pergamon, New York, 1978).
[35] *Handbook of Chemistry and Physics*, 69th ed., edited by R. W. Weast (Chemical Rubber Co., Boca Raton, FL, 1989); *Numerical Data and Functional Relationships in Science and Technology,* edited by O. Madelung, Landolt-Börnstein, New Series, Group III, Vol. 17, Pt. a (Springer, Berlin, 1982).
[36] C. J. Buchenauer, M. Cardona, and F. H. Pollak, Phys. Rev. B **3**, 1243 (1971).
[37] A. Ohtake, H. Omi, and T. Osaka (unpublished).